ENERGY YIELD AND PERFORMANCE RATIO OF III-V ON SILICON DUAL JUNCTION SOLAR CELLS IN DIFFERENT CLIMATE ZONES

Oliver Höhn, Mario Hanser, Marc Steiner, Elke Lorenz, Benedikt Bläsi, Stefan W. Glunz, Frank Dimroth
Fraunhofer Institute for Solar Energy Systems ISE
Heidenhofstr. 2, 79110 Freiburg, Germany

ABSTRACT: The importance of predicting outdoor performance of tandem solar devices is growing, as silicon-based tandem solar cells approach industrialization. A 2-terminal configuration has the advantage of lower parasitic absorption and less electrical wiring at module level as compared to a 4-terminal device. However, a 2-terminal tandem device is sensitive to current-mismatch losses. As a result, there is a strong interest to determine the outdoor energy yield in addition to the STC efficiency in order to evaluate the real impact of current-mismatch losses on the energy yield. We compare the energy yield, harvesting efficiency and performance ratio of a silicon-based dual junction solar cell in 2- and 4-terminal configuration to a silicon single junction device for different locations in the world.
We find that changes due to current mismatch do not lead to a relevant decrease in harvesting efficiency in 2-terminal tandem solar cells and thus are no reason to principally prefer 4-terminal tandem solar cells. The assumption that current mismatch might be a severe issue in 2-terminal tandems does not hold – they show similar performance as silicon single-junction devices. Note that the performance ratio of 4-terminal tandems shows a lower dependence on location than 2-terminal tandems as well as single junction solar cells, and thus for certain locations show an exceptionally high performance ratio.

1 INTRODUCTION

With silicon-based tandem solar cells approaching industrialization, the significance of predicting outdoor performance of tandem solar devices is growing. Compared to a 4-terminal tandem solar cell, a 2-terminal configuration has the advantage of lower parasitic absorption and less electrical wiring at module level. On the other hand, a 2-terminal tandem device design can suffer from current-mismatch losses. As a result, there is a strong interest to determine the outdoor energy yield instead of the standard testing condition (STC) efficiency to evaluate the real impact of current-mismatch losses. Such an analysis of the energy yield is crucial when assessing the potential and the electricity costs of new and emerging PV technologies in comparison to existing technologies.

We compare the energy yield, harvesting efficiency and performance ratio of an $Al_{0.21}Ga_{0.79}As$-on-silicon dual junction solar cell in 2- and 4-terminal configuration to a silicon single-junction device for different locations in the world.

Various models exist to describe energy yield modelling of silicon-based tandem solar cells [1–14]. Those are often limited to one location, idealized solar cells are assumed, temperature effects are neglected, or purely modeled spectra (e.g. by SMARTS2 [15]) are used. Apart from this, most of these investigations model perovskite silicon tandem solar cells.

We use standardized satellite-based data for different climate zones as representatives for different conditions all over the world. With these, the energy yield of 2- and 4-terminal AlGaAs-on-silicon dual junction devices is determined and compared to single-junction devices accounting for temperature effects. Based on this, we investigate if spectral variations lead to significant losses especially in 2-terminal tandem solar cells at different locations.

2 MODELING METHOD

2.1 Spectral Data

We use spectral data and ambient conditions such as temperature from the IEC international standard "Photovoltaic (PV) module performance testing and energy rating – Part 4: Standard reference climatic profiles" [16] that are based on satellite data and represent irradiation in all relevant climate zones (Table 1). We assume fix tilted modules oriented towards the equator (south or north respectively) and a tilt angle that corresponds to the latitude angle. This data is used for performance testing of silicon single-junction solar cells. In [17] the energy yields of AlGaAs-on-Silicon devices between ground-measured and satellite-based data are compared for Golden, Co, USA. It was shown that the difference in yield is below 1%. That study is restricted to just one location and therefore the overall accuracy of energy yield calculations based on satellite data cannot be estimated exactly. However, for technology comparison (e.g. single-junction vs dual-junction) a difference between satellite-based data and ground measured data does not have to be a problem. We do compare energy yields for different technologies for different locations, i.e different spectral irradiance, but the perfectly accurate absolute values are not the focus. Thus, satellite-based data are suitable for this purpose.

Table 1 For the 6 investigated climate zones the total annual irradiance, the average photon energy APE (307-1200nm (1.80 for AM1.5g)) and the mean temperature are summarized together with the latitude at which the spectral data was recorded.

	Irradiance [kWh/m^{2}a]	Latitude	APE [eV]	Mean T [K]
tropical humid	1759	1°S	1.87	298.6
temperate continental	1307	33°N	1.81	281.2
subtropical coastal	1475	33°N	1.84	291.2
subtropical arid	2345	56°N	1.82	295.5
High elevation	2202	34°N	1.8	271.1
temperate coastal	956	57°N	1.82	283.8

2.2 Modeled Device

As modelled device we assume a module stack consisting of a PERC-like silicon bottom solar cell including rear random pyramids with a rear reflector made from a stack of silicon oxide and silver. The silicon solar cell front side is well passivated and planar. On top a highly performing AlGaAs solar cell is assumed to be monolithically integrated (e.g. by direct growth or bonding). On top of the solar cell a single layer tantalum oxide ARC minimizes reflection between the top cell and the front encapsulation (EVA/glass stack). The front glass has an ARC with a refractive index of 1.3 (See **Figure 1**). We call this type of device, where contacts, cell distances, partial shading, cell interconnection and other module-related effects are neglected, a module stack. In other words, we account for the module glass, as this has a relevant optical influence when modelling yield, but for the purpose of technology comparison, we neglect other effects that are not directly linked to the technology.

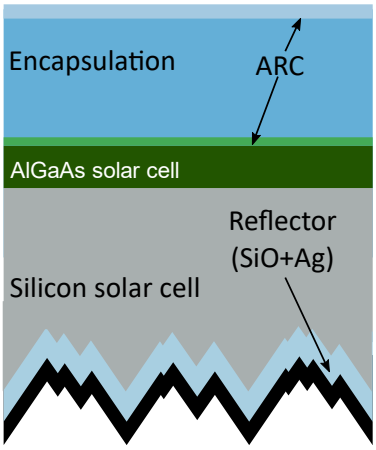

Figure 1 Sketch of the modeled silicon based tandem device.

In the case of the 2-terminal device, the cells are assumed to be interconnected in series. For the 4-terminal result the same sub cell EQEs are assumed. The IVs are modeled separately, and the efficiencies are added up. This results in an overestimation of the 4-terminal efficiency. Usually, the required additional interface will create additional optical losses. The additional contacts in-between will add resistive losses, additional shading and parasitic absorption. As these losses depend severely on the exact design, we decided to neglect them in the quantitative analysis, and account for them qualitatively in the conclusions.

The electrical parameters of the relevant device with $Al_{0.225}Ga_{0.775}As$ are shown in Table 2 and the resulting cell performance at standard test conditions in Table 3

Table 2. Cell parameters of the $Al_{0.225}Ga_{0.775}As$ top junction and the silicon bottom junction used in the temperature dependent two diode model. The values are given for a temperature of T = 298 K.

	$Al_{0.225}Ga_{0.775}As$	Si
J_{01} **[mA/cm²]**	6.75e-21	1.4e-10
J_{02} **[mA/cm²]**	0	2e-6
R_s **[Ω cm²]**	0.103	0.05
R_p **[Ω cm²]**	10 000	30 000
E_g **[eV]**	1.73	1.12

Table 3 Open circuit voltage V_{oc}, short circuit current J_{sc} as well as fill factor FF and efficiency η_{stc} at standard test conditions are summarized. For the sake of comparison, the silicon cell is also shown as a single junction device assuming front side pyramids. In case of the tandem device all results are additionally shown for the top and bottom junction separately. The STC efficiency of the 4-terminal tandem is given by the sum of the top and bottom cell efficiency.

	Single Junction	Top	Bot	2-terminal-Tandem
V_{oc} **[V]**	0.68	1.29	0.66	1.95
J_{sc} **[mA/cm²]**	41.9	19.4	21.7	19.4
FF [%]	84	90	83	90
η_{stc} **[%]**	23.8	22.5	11.9	34.0

Note that the shown 2-terminal tandem device is not current matched at STC. On average, the spectra of the reference regions are slightly blue shifted, compared to AM1.5g and the operating temperature is significantly higher than 298 K. The investigated device is optimized for these conditions.

The band gap of the optimal 2- and 4-terminal tandem solar cell in terms of yield are very close to each other, which allows a comparison of 2- and 4-terminal configurations with the same top cell. For detailed explanation why this device is optimal see section 3.1.

2.3 Two diode modeling

The electrical model is based on a temperature dependent 2-diode model for each subcell including series and parallel resistance R_s and R_p. The 2-diode equation is an implicit equation for the current density of a solar cell

$$J = J_{ph} - J_{01}\left\{\exp\left(\frac{q(V-JR_s)}{k_B T}\right) - 1\right\} - J_{02}\left\{\exp\left(\frac{q(V-JR_s)}{2k_B T}\right) - 1\right\} - \frac{V-JR_s}{R_p}, \quad (1)$$

depending on the voltage V, the incoming photo current density J_{ph}, the dark saturation currents J_{01} and J_{02} and the Temperature T, where q is the elementary charge and k_B the Boltzmann constant. The saturation currents temperature dependence is described by the Wanlass model [18]:

$$J_{01} = \beta_{01} T^3 \exp\left(-\frac{E_g(T)}{k_B T}\right), \quad (2)$$

$$J_{02} = A_{01} \exp\left(B_{01} E_g(T)\right) T^{5/2} \exp\left(-\frac{E_g(T)}{k_B T}\right), \quad (3)$$

with the Wanlass parameters β_{01} and A_{01} and the band gap $Eg(T)$. The Varshni relation [19]

$$E_g(T) = E_0 - \frac{\alpha T^2}{T+\beta} \quad (4)$$

describes the temperature dependence of the band gap with the material constants $\alpha = 4.73$e-4 and $\beta = 636$ as well as the band gap at absolute zero $E_0 = 1.166$eV for silicon taken from [20]. In case of the AlGaAs top junction the temperature dependence of the band gap is calculated with binary and tertiary material parameters reported by Vurgaftmann [21]. For both solar cells the Wanlass parameters β_{01} and A_{01} and J_{02} parameter A_{01} and B_{01} are extracted at an initial temperature $T = 298$ K, with the corresponding band gap $E_g(T)$ from the J_{01} and J_{02} values shown in Table 2.

Within this study we assume the following empirical

relation between the ambient temperature T_{amb} and the module temperature T as given by [22]

$$T = I \cdot 0.025 \frac{\mathrm{m^2K}}{\mathrm{W}} + T_{\mathrm{amb}}, \qquad (5)$$

where I is the global irradiance power on the module plane. All input parameters for the $Al_{0.225}Ga_{0.775}As$ composition as well as the silicon junction are listed in Table 2 for a temperature of T = 298 K. The value 0.025m²K/W is an empirical value that represents a ground-mounted PV power plant. We use the same values for both the single junction and the tandem device. In the end the higher efficiency of the tandem device will lead to a lower temperature increase. However, this is a minor effect, which is neglected in this study and will further boost both the 4-terminal and 2-terminal tandem performance ratio.

The temperature coefficient dV_{oc}/dT is calculated as the slope of the V_{oc} curves in Figure 2. For the silicon solar cell the values -2.1 mV/K as part of the tandem device with J_{sc} = 21.7 mA/cm², and -2 mV/K for the single junction under AM1.5g with J_{sc} = 42.1 mA/cm² are in good agreement with earlier publications [23], which reported a temperature coefficient of -2.1 mV/K for the silicon device. Thus, we can assume that the Wanlass model and the J_{02} model that was originally developed for III-V-solar cells reasonably reproduces the temperature dependence of the silicon bottom solar cell.

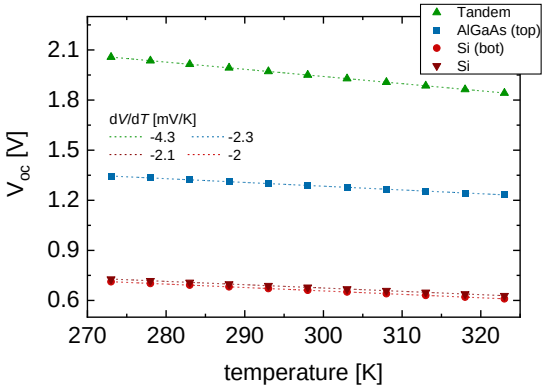

Figure 2 The open-circuit voltage V_{oc} is plotted over the temperature ***T*** for the silicon single junction device at a short circuit current of J_{sc} = 41.9 mA/cm², as well as for the top and bottom junction of a tandem device consisting of $Al_{0.225}Ga_{0.775}As$ and silicon. The short-circuit currents in this case are J_{sc} = 19.4 mA/cm² and J_{sc} = 21.7 mA/cm² for the top and bottom junction, respectively. The slope of these curves correlates with the temperature coefficients supporting the chosen model for the temperature depended band gaps.

The temperature and angle of incidence-dependent EQE is modelled using the OPTOS formalism [8, 24, 25]. In this manner, the impact of cell temperature, as well as the incident angle of the solar radiation on the solar cell power output is considered. Effects of the temperature and the incidence angle on the EQE are depicted in **Figure 3** and **Figure 4**, respectively.

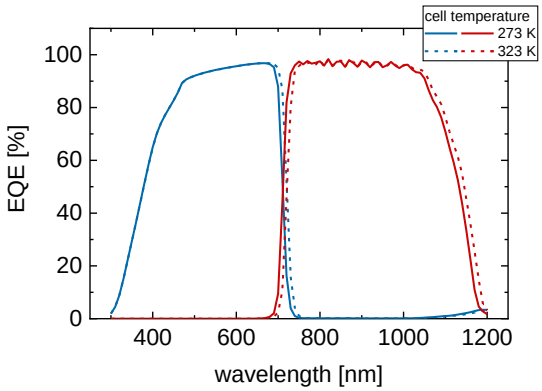

Figure 3 The EQE of the investigated tandem device with a $Al_{0.225}Ga_{0.775}As$ composition as top cell and a silicon bottom cell is plotted for two different temperatures. The top cell EQE's are depicted in blue and the bottom cell EQE's in red. A shift of the total EQE is observed towards higher wavelength for increasing temperature.

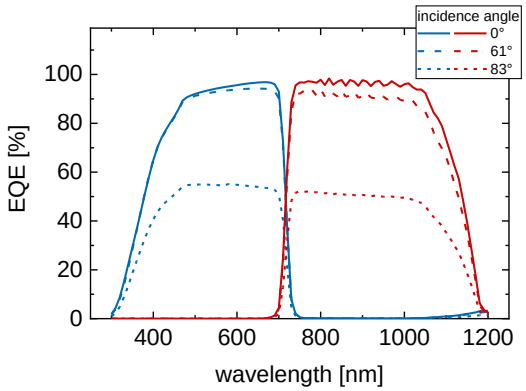

Figure 4 Investigated is the EQE's angle dependence of a tandem device with a $Al_{0.225}Ga_{0.775}$. As composition as top cell and a silicon bottom cell. It was found, that the EQE change with incoming angle is very small for low incoming angles. For higher angles, starting at approximately *60°*, the EQE begins to drop drastically.

2.4 Energy yield modeling

The used model for the determination of the energy yield (YieldOpt) is described in more detail in [5, 8, 17]. It combines the above mentioned spectral and ambient data from the specific locations, the 2-diode-models for the cells and the temperature and angle dependent EQE into one single modelling tool.

The energy yield is calculated in 6 different climate zones. 2- and 4-terminal dual junction solar cells are compared with a silicon solar cell in terms of harvesting efficiency (Annual Energy Output divided by Annual Incident Energy) and performance ratio (harvesting efficiency divided by STC efficiency).

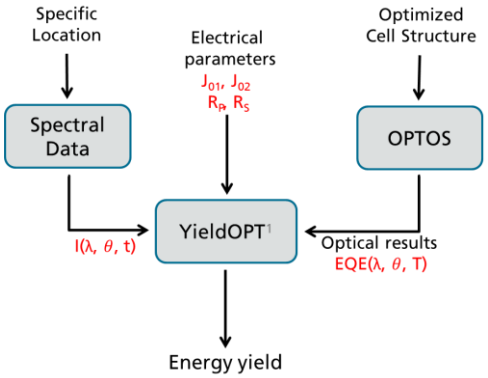

Figure 5 Sketch of the simulation formalism.

3 RESULTS AND DISCUSSION

3.1 Variation of top cell band gap

As a first step the harvesting efficiency was modeled for the locations from the IEC international standard [16] for a 2- and 4-terminal $Al_xGa_{1-x}As$-silicon-tandem solar cell with different Al-content X, to vary the top cell band gap (Figure 6). The Wanlass parameter extracted from the saturation current J_{01} in Table 2 were used for all top cells to simulate a constant cell quality.

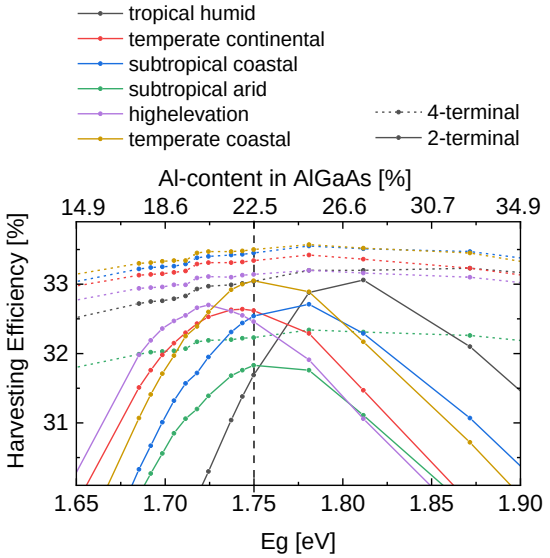

Figure 6 Harvesting efficiency for an $Al_xGa_{1-x}As$-on-silicon solar cell for different Al-content x and different locations.

The harvesting efficiency of the 4-terminal device shows only a very weak dependence on the band gap. Thus, a device with one single Al-content will be perfectly suitable for every location. The 2-terminal tandem shows a dependence of harvesting efficiency on band gap and especially the optimal band gap depends on the location. However, as for an industrialization the aim is, to produce only one single device, we decided to compare 2- and 4-terminal yield for one device with an Al-content of x=22.5%. This composition leads to good harvesting efficiencies considering the 2-terminal performance in all climate zones and is at the same time very close to the optimal working point of the 4-terminal solar cell. Thus, a fair comparison between the 2 device-configurations is possible with the selected top cell.

3.2 Results of the optimal device

In the following we have a more detailed look at the optimal device, build of an $Al_{0.225}Ga_{0.775}As$ top and a silicon bottom solar cell.

The harvesting efficiency (Figure 7) of both tandem devices is significantly higher than the harvesting efficiency of the single junction solar cell. The 4-terminal device shows the highest harvesting efficiency, with the median 0.5% absolute above the 2-terminal cell median value. Note that additional losses in the 4-terminal device as mentioned in section 2.2 are neglected, meaning that this gain will most likely vanish or even be overcompensated depending on the exact design of the 4-terminal interconnection.

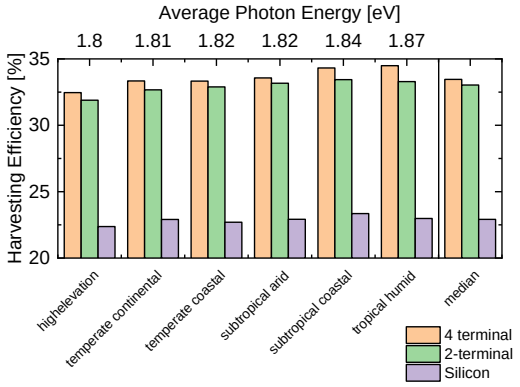

Figure 7 Harvesting efficiency (Annual Energy Output divided by Annual Incident Energy) of the 3 investigated devices for different climate zones.

While the performance ratio PR (PR is given as the harvesting efficiency divided by the STC efficiency) of the 2-terminal and 4-terminal device show similar performance for the locations with APE 1.8-1.82eV, the PR of the 4-terminal device for high APE regions (subtropical costal and tropical humid) is higher (see Figure 8). Thus, the median of the PR of the 4-terminal tandem is higher by 1.0%. This explains the above mentioned slightly higher harvesting efficiency of the 4-terminal device as compared to the 2-terminal configuration. Note that the STC efficiencies of the 4- and 2-terminal device in this optimized system are very similar (2-terminal: 34%, 4-terminal 34.4%).

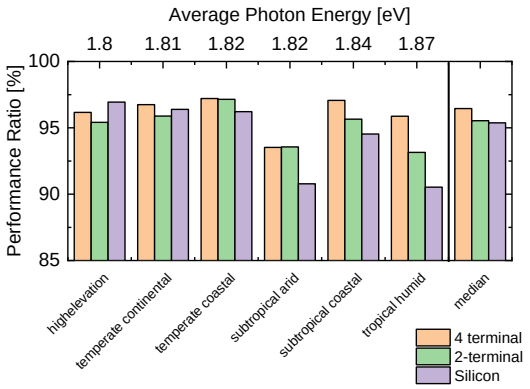

Figure 8 Performance ratio (Harvesting Efficiency divided by STC Efficiency) of the three investigated devices for different climate zones.

One can see that the PR depends on the average photon energy APE (APE describes the overall power in the

spectrum divided by overall number of photons per second) for the 2-terminal tandem and the silicon single junction in almost the same way (see Figure 9). The PR of the 4-terminal tandem device shows a lower dependence on the average photon energy. The PR of a 2-terminal tandem could be further improved by adjusting the top cell band gap to the APE. However, this would significantly increase the effort in production and might not be feasible. Note that the median performance of the 2-terminal tandem device is as good as for the pure silicon cell. Only the 4-terminal tandem performs particularly well in certain locations.

The lower points at APE=1.82 eV belong to the "subtropical arid" climate zone, where very high temperatures occur. As the silicon single-junction solar cell has a larger relative voltage temperature coefficient, it loses more in efficiency than the 2- and 4-terminal tandem devices. Consequently, the PR of the single junction is decreased stronger due to the high temperatures. When comparing the two locations with an APE of 1.82eV, it is observed that the temperature can have a severe effect to the performance ratio. This occurs for 2- and 4-terminal tandem cells in a very similar way.

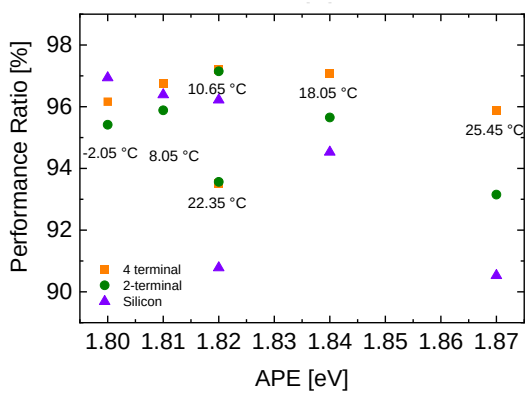

Figure 9 Performance ratio of the three investigated devices depending on the average photon energy The points are labeled with the average ambient temperature derived from the satellite data (only during daytime, as the night temperature has no influence on the device performance).

The calculation was repeated for a constant module temperature of T=298K, to prove that the difference in PR at an APE of 1.82 eV is simply caused by temperature effects and not just by different spectral influences of spectra with the same mean APE. One can see that the devices at the two locations with an APE of 1.82 eV behave very similar, when neglecting temperature effects. This proofs that the difference in the performance ratio of these two locations is mainly caused by temperature effects. It also hints towards APE in combination with ambient temperature being a good indicator for the performance ratio of this type of dual-junction solar cell.

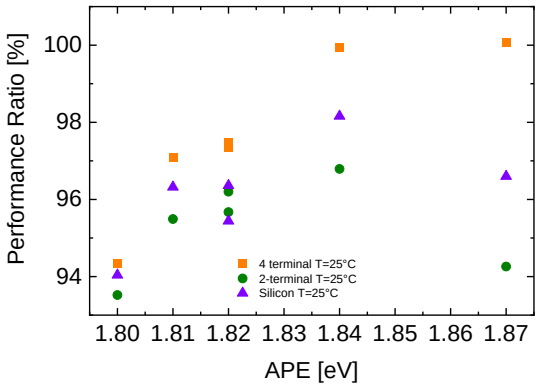

Figure 10 Performance ratio of the three investigated devices depending on the average photon energy for an assumed module temperature of *298* K.

Summarized, we find that the PR of well-designed 2-terminal III-V-on-silicon dual junction solar cells behave like the PR of silicon single junction solar cells. There are no relevant changes in the PR due to spectral variations that only occur in the 2-terminal dual junction but not in the single junction device. We show that this holds for all investigated climate zones. Thus, the STC efficiency gain of well-designed 2-terminal III-V-on-silicon dual junction solar cells will translate to nearly the same gain in energy harvesting efficiency.

It was also found that the PR of 4-terminal tandem solar cells (assuming the same EQE and IVs and no additional losses) is principally higher than the 2-terminal device PR. This is especially true for locations with high APE. However, this gain (~1% in median) will be mostly compensated by the neglected additional losses e.g. due to reflection at additional interfaces and losses due to more complex electrical wiring. Thus, well designed 2-terminal and 4-terminal devices will show similar harvesting efficiencies under outdoor conditions. In such a device the PR of a 2-terminal tandem is well comparable to the PR of a silicon single junction solar cell.

When comparing these results to temperature-independent calculations, i.e. temperature is set to *298* K, one observes that the module temperature can have a relevant effect on the performance ratios. The single-junction solar cell has a larger temperature coefficient than the tandem device. Thus, the performance ratio of the single junction is boosted at very cold locations, while the PR of the tandems behaves better at rather warm locations. At locations with very high APE (>1.84eV), that are typically warm, the slight impairment from current mismatch in 2-terminal tandems is compensated by the better temperature coefficient as compared to single junction solar cells.

4 CONCLUSION

We showed that spectral changes due to current mismatch do not lead to a relevant decrease in harvesting efficiency in 2-terminal III-V-on-silicon dual-junction solar cells. The assumption that current mismatch might be a severe issue in 2-terminal tandems does not hold for the investigated devices – they show similar performance as silicon single-junction devices. Note that the PR of 4-terminal tandems shows a lower dependence on location than 2-terminal tandems as well as single junction solar cells, and thus benefits at certain locations

5 ACKNOWLEDGEMENTS

This work was supported in part by the European Union's Horizon 2020 Research and Innovation Program within the Project SiTaSol under Grant 727497

6 REFERENCES

[1] I. M. Peters, H. Liu, T. Reindl, and T. Buonassisi, "Global Prediction of Photovoltaic Field Performance Differences Using Open-Source Satellite Data," *Joule*, vol. 2, no. 2, pp. 307–322, 2018.

[2] J. Lehr, M. Langenhorst, R. Schmager, S. Kirner, U. Lemmer, B. S. Richards, C. Case, and U. W. Paetzold, "Energy yield modelling of perovskite/silicon two-terminal tandem PV modules with flat and textured interfaces," *Sustainable Energy Fuels*, vol. 8, p. 506, 2018.

[3] M. T. Hörantner and H. J. Snaith, "Predicting and optimising the energy yield of perovskite-on-silicon tandem solar cells under real world conditions," *Energy & Environmental Science*, vol. 10, no. 9, pp. 1983–1993, 2017.

[4] M. Jošt, E. Köhnen, A. Morales Vilches, B. Lipovšek, K. Jäger, B. Macco, A. Al-Ashouri, J. Krc, L. Korte, B. Rech, R. Schlatmann, M. Topic, B. Stannowski, and S. Albrecht, "Textured interfaces in monolithic perovskite/silicon tandem solar cells: Advanced light management for improved efficiency and energy yield," *Energy & Environmental Science*, vol. 11, no. 12, pp. 3511–3523, 2019.

[5] M. Steiner, G. Siefer, T. Hornung, G. Peharz, and A. W. Bett, "YieldOpt, a model to predict the power output and energy yield for concentrating photovoltaic modules," *Prog. Photovolt: Res. Appl.*, vol. 23, no. 3, pp. 385–397, 2015.

[6] H. Schulte-Huxel, T. J. Silverman, M. G. Deceglie, D. J. Friedman, and A. C. Tamboli, "Energy Yield Analysis of Multiterminal Si-Based Tandem Solar Cells," *IEEE J. Photovoltaics*, pp. 1–8, 2018.

[7] R. Schmager, M. Langenhorst, J. Lehr, U. Lemmer, B. S. Richards, and U. W. Paetzold, "Methodology of energy yield modelling of perovskite-based multi-junction photovoltaics," *Opt. Express*, vol. 27, no. 8, A507, 2019.

[8] N. Tucher, O. Höhn, J. N. Murthy, Martinez, J. C. Steiner, M., A. Armbruster, E. Lorenz, B. Bläsi, J. C. Goldschmidt, N. Tucher, O. Höhn, J. C. Martinez, M. Steiner, B. Bläsi, and J. C. Goldschmidt, "Energy yield analysis of textured perovskite silicon tandem solar cells and modules," *Optics Express*, vol. 27, no. 20, A1419, 2019.

[9] E. F. Fernández, D. L. Talavera, F. M. Almonacid, and G. P. Smestad, "Investigating the impact of weather variables on the energy yield and cost of energy of grid-connected solar concentrator systems," *Energy*, vol. 106, pp. 790–801, 2016.

[10] D. Dirnberger, G. Blackburn, B. Müller, and C. Reise, "On the impact of solar spectral irradiance on the yield of different PV technologies," *Solar Energy Materials and Solar Cells*, vol. 132, pp. 431–442, 2015.

[11] Y. Boose, C. Heller, O. Stern, and M. Lynass, "The Effect of Spectral Mismatch on the Annual Energy Output of CdTe-, CIGS- and Si-Based Photovoltaic Modules," (eng), 2012.

[12] M. Alonso-Abella, F. Chenlo, G. Nofuentes, and M. Torres-Ramírez, "Analysis of spectral effects on the energy yield of different PV (photovoltaic) technologies: The case of four specific sites," *Energy*, vol. 67, pp. 435–443, 2014.

[13] H. Liu, Z. Ren, Z. Liu, A. G. Aberle, T. Buonassisi, and I. M. Peters, "The realistic energy yield potential of GaAs-on-Si tandem solar cells: a theoretical case study," *Opt. Express*, vol. 23, no. 7, pp. A382, 2015.

[14] O. Dupré, B. Niesen, S. de Wolf, and C. Ballif, "Field Performance versus Standard Test Condition Efficiency of Tandem Solar Cells and the Singular Case of Perovskites/Silicon Devices," (eng), *The Journal of Physical Chemistry Letters*, pp. 446–458, http://pubs.acs.org/doi/pdf/10.1021/acs.jpclett.7b02277, 2018.

[15] C. Gueymard, "SMARTS2, A Simple Model of the Atmospheric Radiative Transfer of Sunshine," Florida Solar Energy Center. University of Central Florida, Cocoa, FL, USA, 1995.

[16] *Photovoltaic (PV) module performance testing and energy rating – Part 4: Standard reference climatic profiles*, 61853-4, 2018.

[17] O. Höhn, J. N. Murthy, M. Steiner, N. Tucher, E. Lorenz, J. C. Goldschmidt, F. Dimroth, and B. Blasi, "Impact of Irradiance Data on the Energy Yield Modeling of Dual-Junction Solar Module Stacks for One-Sun Applications," *Photovoltaics, IEEE Journal of*, vol. 11, no. 3, pp. 692–698, 2021.

[18] M. W. Wanlass, K. A. Emery, T. A. Gessert, G. S. Horner, C. R. Osterwald, and T. J. Coutts, "Practical considerations in tandem cell modeling," *Solar Cells*, vol. 27, no. 1-4, pp. 191–204, 1989.

[19] Y. P. Varshni, "Temperature dependence of the energy gap in semiconductors," *Physica*, vol. 34, no. 1, pp. 149–154, 1967.

[20] P. Singh, S. Singh, M. Lal, and M. Husain, "Temperature dependence of I–V characteristics and performance parameters of silicon solar cell," *EuroSun2004*, vol. 92, no. 12, pp. 1611–1616, 2008.

[21] I. Vurgaftman, J. R. Meyer, and L. R. Ram-Mohan, "Band parameters for III–V compound semiconductors and their alloys," *J. Appl. Phys.*, vol. 89, no. 11, p. 5815, 2001.

[22] E. Barykina and A. Hammer, "Modeling of photovoltaic module temperature using Faiman model: Sensitivity analysis for different climates," *Sol Energy*, vol. 146, pp. 401–416, 2017.

[23] S. Bensalem, M. Chegaar, and M. Aillerie, "Solar Cells Electrical Behavior under Thermal Gradient," *Energy Procedia*, vol. 36, pp. 1249–1254, 2013.

[24] N. Tucher, J. Eisenlohr, P. Kiefel, O. Höhn, H. Hauser, I. M. Peters, C. Müller, J. C. Goldschmidt, and B. Bläsi, "3D optical simulation formalism OPTOS for textured silicon solar cells," *Opt. Express*, vol. 23, no. 24, pp. A1720, 2015.

[25] N. Tucher, J. Eisenlohr, H. Gebrewold, P. Kiefel, O. Höhn, H. Hauser, J. C. Goldschmidt, and B. Bläsi, "Optical simulation of photovoltaic modules with multiple textured interfaces using the matrix-based formalism OPTOS," *Optics Express*, vol. 24, no. 14, pp. A1083, 2016.